ASME Accepted Manuscript Repository

Institutional Repository Cover Sheet

Martin	Berthold
First	*Last*

ASME Paper Title: Towards Investigation of External Oil Flow from a Journal Bearing in an Epicyclic Gearbox

Authors: Martin Berthold, Hervé Morvan, Richard Jefferson-Loveday, Colin Young

ASME Journal Title: Journal of Engineering for Gas Turbines and Power

Volume/Issue Unknown** Date of Publication (VOR* Online) Unknown**

ASME Digital Collection URL: Unknown**

DOI: Unknown**

** The journal paper is not yet listed online.

*VOR (version of record)

GTP-17-1410

TOWARDS INVESTIGATION OF EXTERNAL OIL FLOW FROM A JOURNAL BEARING IN AN EPICYCLIC GEARBOX

Martin Berthold
Gas Turbine and Transmissions Research Centre (G2TRC), University of Nottingham, Nottingham, UK

Prof. Hervé Morvan
Gas Turbine and Transmissions Research Centre (G2TRC), University of Nottingham, Nottingham, UK

Dr. Colin Young
Rolls-Royce plc
Derby, UK

Dr. Richard Jefferson-Loveday
Gas Turbine and Transmissions Research Centre (G2TRC), University of Nottingham, Nottingham, UK

ABSTRACT

High loads and bearing life requirements make journal bearings the preferred choice for use in high power, epicyclic gearboxes in jet engines. In contrast to conventional, non-orbiting journal bearings in epicyclic star gearboxes, the kinematic conditions in epicyclic planetary arrangements are much more complex. With the planet gears rotating about their own axis and orbiting around the sun gear, centrifugal forces generated by both motions interact with each other and affect the external flow behavior of the oil exiting the journal bearing.

This paper presents a literature and state-of-the-art knowledge review to identify existing work performed on cases similar to external journal bearing oil flow. In order to numerically investigate external journal bearing oil flow, an approach to decompose an actual journal bearing into simplified models is proposed. Later, these can be extended in a step-wise manner to allow key underlying physical phenomena to be identified. Preliminary modeling considerations will also be presented. This includes assessing different geometrical inlet conditions with the aim of minimizing computational requirements and different numerical models for near-wall treatment. The correct choice of near-wall treatment models is particularly crucial as it determines the bearing's internal and external thermal behavior and properties. The findings and conclusions are used to create a three dimensional (3D), two-component computational fluid dynamic (CFD) sector model with rotationally periodic boundaries of the most simplistic approximation of an actual journal bearing: a non-orbiting representation, rotating about its own axis, with a circumferentially constant, i.e. concentric, lubricating gap. The inlet boundary conditions for simulating the external oil flow are generated by partly simulating the internal oil flow within the lubricating gap. In order to track the phase interface between the oil and the air surrounding the bearing, the Volume of Fluid (VoF) method is used. The quality of the CFD simulations of the domain of interest is not only dependent on the accuracy of the inlet conditions, but is also dependent on the computational mesh type, cell count, cell shape and numerical methods used. External journal bearing oil flow was simulated with a number of different mesh densities and the effect on the flow field behavior will be discussed. Two different operating temperatures, representing low and high viscosity oil, were used and their effect on the flow field behavior will also be assessed.

In order to achieve the future objective of creating a design tool for routine use, key areas will be identified in which further progress is required. This includes the need to progressively increase the model fidelity to eventually simulate an orbiting journal bearing in planetary configuration with an eccentric, i.e. convergent-divergent, lubricating gap.

INTRODUCTION

A step change in jet engine efficiency can be achieved by decoupling the fan from its driving turbine. The key technology to enable this advance is an epicyclic reduction gearbox (Figure 1).

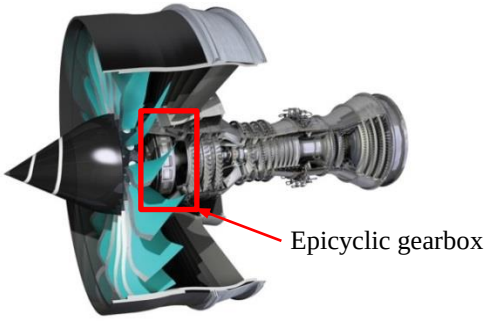

Figure 1: Rolls-Royce Ultrafan™ engine with epicyclic gearbox [1].

Based on their achievable gear ratios, for use in jet engines, both the so-called star and planetary configuration are viable options (Figure 2 and Figure 3).

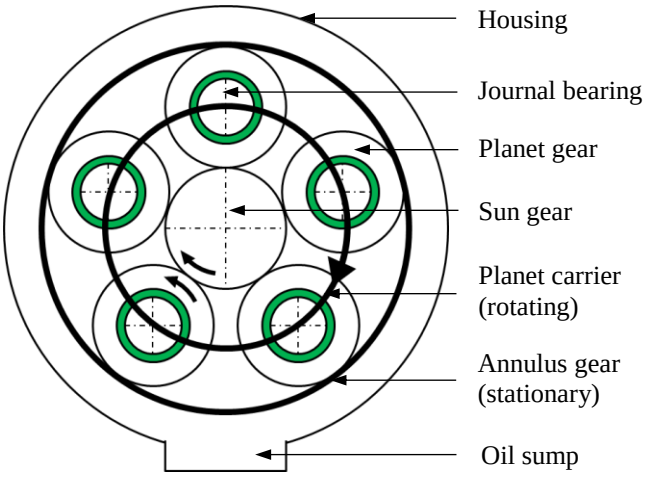

Figure 2: Epicyclic gearbox in planetary configuration.

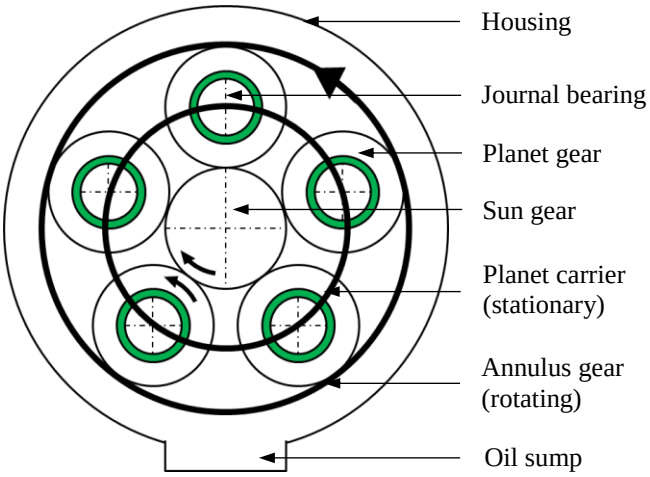

Figure 3: Epicyclic gearbox in star configuration.

Due to the very high loads transmitted by the gearbox, even a small power loss leads to significant generation of heat. In order to remove this heat, substantial quantities of coolant are required, a large amount of which is supplied to the planet bearings [2]. Effective and efficient flow path management is therefore essential. Failure to design an effective oil scavenge system can lead to a number of issues.

a) Increased momentum exchange between the rotating parts and the oil, causing momentum losses or churning, will adversely affect gearbox efficiency.
b) The risk of gearbox flooding increases. This may cause the planet gears to dip into an oil bath when orbiting around the sun gear, leading to a drastic increase in power loss.
c) Oil presence in hot areas of the gearbox for a long period of time may cause the oil temperature to increase beyond acceptable limits, leading to premature oil degradation and wear.

In order to ensure reliable gearbox operation and maximum oil scavenge effectiveness, a comprehensive understanding is required of the oil flow behavior as it exits the journal bearing. The long term objective of this research project is to develop an understanding of how the oil exiting the journal bearing interacts with the air and the components surrounding the domain of interest and how the flow behavior is affected by geometrical and operational parameters. Additionally, this work aims to provide boundary conditions for a larger CFD model which simulates the oil scavenge flow between the annulus gear and the gearbox housing (Figure 2, Figure 3).

NOMENCLATURE

2D	Two dimensional
3D	Three dimensional
CFD	Computational Fluid Dynamics
DPM	Discrete Phase Model
LS	Level-Set
MTO	Maximum Take-Off
SPH	Smoothed Particle Hydrodynamics
SST	Shear Stress Transport
VoF	Volume of Fluid
d	Diameter [m]
$d_{g,i}$	Inner gear diameter [m]
h	Liquid film thickness [m]
h/h_0	Relative lubricating gap height [-]
h_0	Lubricating gap height [m]
k	Turbulent kinetic energy [J/kg]
l_{free}	Free inlet length [m]
l_{total}	Total inlet length [m]
$N_{cells,2D}$	Number of cells (2D) [-]
$N_{cells,oil,d1}$	Number of cells across oil film at location d_1 [-]
$N_{cells,total}$	Total number of cells [-]
$N_{cells,\phi}$	Number of cells in the circumferential direction [-]
N_{lig}	Number of ligaments [-]
Oh	Ohnesorge number [-]
r	Radius [m]
Re	Reynolds number [-]
Re_{crit}	Critical Reynolds number [-]
St	Stability number [-]
Ta	Taylor number [-]
T	Temperature [°C]
t	Time [s]
t_1	Height of first cell perpendicular to wall [mm]
$\dot{V}$	Oil volume flow rate [m^3/s]
$\dot{V}^+$	Non-dimensional oil volume flow rate [-]
$\dot{V}_1^+$	Non-dimensional transition oil volume flow rate from direct droplet to ligament formation [-]
$\dot{V}_2^+$	Non-dimensional transition oil volume flow rate from ligament to sheet formation [-]
We	Weber number [-]
We^*	Modified Weber number [-]
x	Coordinate of position [m]

ε	Turbulent dissipation rate [m^2/s^3]
ρ	Liquid density [kg/m^3]
μ	Liquid viscosity [kg/(ms)]
Ω	Angular velocity [rad/s]
ω	Specific dissipation rate [1/s]
σ	Surface tension [N/m]

ANALYSIS APPROACH

The proposed analysis approach is to decompose the journal bearing in the complex environment of an epicyclic planetary gearbox (Figure 2) into simpler models. In its most basic form a journal bearing can be modeled by two concentric cylinders, creating an axially and circumferentially constant lubricating gap height h_0 (Figure 4).

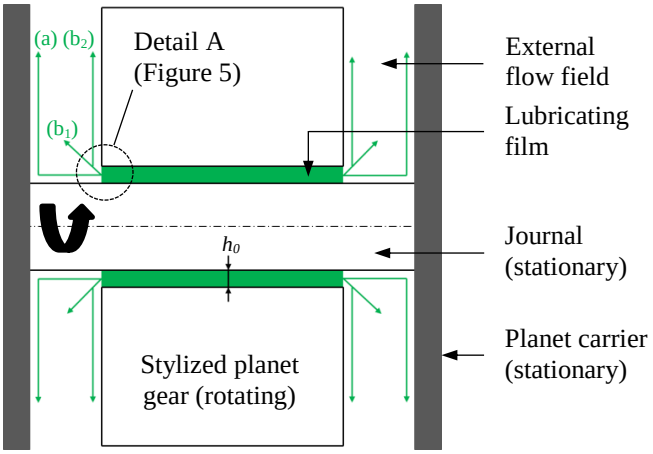

Figure 4: Simple journal bearing model with axially and circumferentially constant lubricating gap height h_0 and possible exit flow directions (a, b).

It is proposed to extend this simple model in a step-wise manner to later include radial gear eccentricity, created by external gear forces, and the orbiting motion of the planet gears, due to planet carrier rotation, to fully represent the kinematic conditions in an epicyclic planetary gearbox. This allows key underlying physical phenomena to be identified.

THEORETICAL FLOW FIELD

Considering the simplified case shown in Figure 4, the domain of interest reduces to a rotor/stator cavity. Due to the importance of this cavity type in the secondary air system of compressors and turbines, extensive analytical, experimental and numerical investigations have been carried out with single-phase air flow. As a result, the air flow pattern is well understood. Most notably, research with single-phase air flow over a free rotating disk was carried out by [3]. Fundamental investigations of enclosed disk systems have been carried out by [4], [5] and [6].

Rotor/stator systems can be classified into systems with and without superimposed radial flows [6]. Generally, flow structures with a superimposed flow component are more complex than those observed in fully enclosed systems. The work of [6] characterizes different flow patterns depending on the cavity configuration, but is also limited to single-phase air flow. Considering the case of oil exiting a journal bearing, the domain of interest (Figure 4) can, in fact, be treated as a rotor/stator cavity with superimposed mass flow. However, the flow field structure developing in the domain of interest is very much dependent on the oil flow regime, e.g. droplets, ligaments, sheets, film or foam, and its characteristics. The flow behavior will also be driven by displacement of the lighter flow component by the denser one.

Depending on the oil's momentum, viscosity, density and surface tension, the following two principle flow paths can occur. Oil exiting the lubricating gap:-

a) does not attach to the rotating gear and travels axially along the journal surface towards the planet carrier (flow path (a) in Figure 5) or
b) does attach to the rotating gear and is subsequently driven radially outward along the gear contour due to the centrifugal force (flow path (b) in Figure 5).

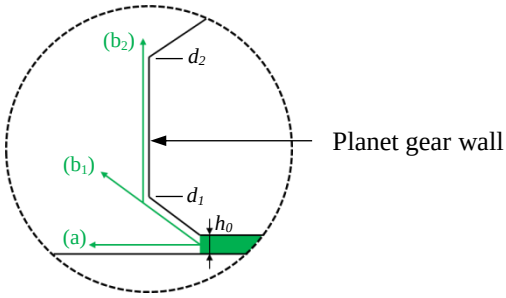

Figure 5: Detail A of planet gear (Figure 4) with possible exit flow directions (a, b).

Naturally, depending on the specific oil properties, the exiting flow can exhibit any combination of the behavior of the two limiting cases described above.

With low axial momentum and high internal fluid friction, i.e. high viscosity, it is anticipated that the fluid's axial velocity reduces rapidly when exiting the lubricating gap. The film thickness will consequently increase. If it increases to an extent where the effects of body forces can no longer be neglected [7], the centrifugal force caused by the swirling motion of the fluid will drive it radially outward. Thus, it will attach to the planet gear chamfer from where it will follow the gear contour (flow path (b) in Figure 5). In this case, the flow essentially behaves like the flow over a rotating cup or disk, which has been subject to analysis on numerous occasions.

STATE-OF-THE-ART KNOWLEDGE REVIEW

Fundamental studies of liquid disintegration by spinning cups were performed by [8], [9] and [10]. The investigations concluded that, with increasing liquid flow rate and/or increasing rotational speed of the cup, the following disintegration regimes can be observed (Figure 6).

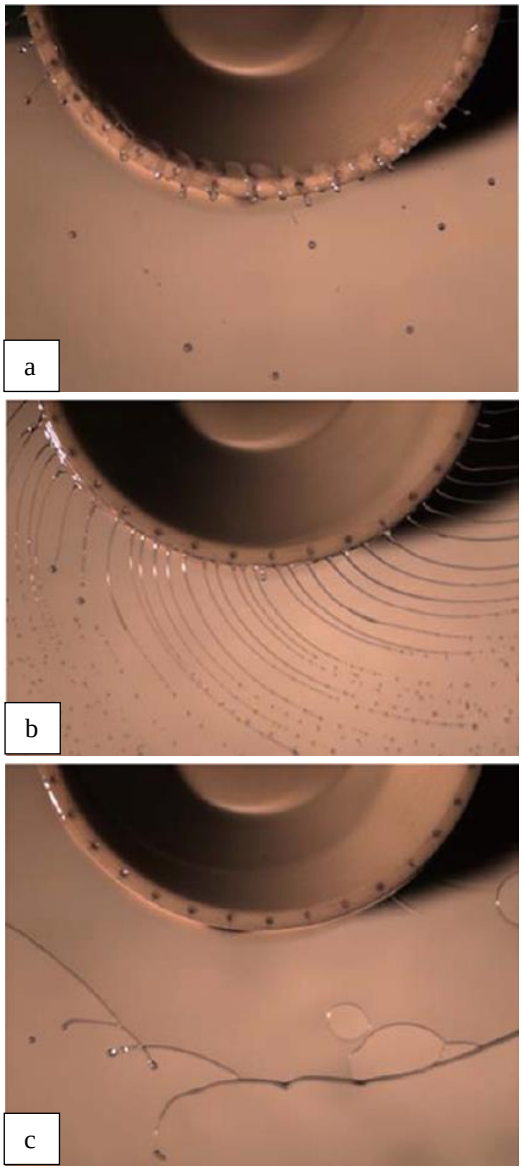

Figure 6: Liquid disintegration from a rotating cup with d=128 mm and the following liquid properties: ρ=1,170 kg/m^3, σ=0.0488 N/m and μ=0.072 kg/(ms) according to [10].
(a) direct droplet formation, Ω=30.06 rad/s, $\dot{V}$=0.00249 l/s
(b) ligament formation, Ω=45.95 rad/s, $\dot{V}$=0.0235 l/s
(c) sheet formation, Ω=67.05 rad/s, $\dot{V}$=0.0235 l/s

Disintegration occurs when surface tension and viscous forces are overcome by centrifugal forces. At high peripheral velocities, this process is aided by the aerodynamic action of the atmosphere [8].

Hinze and Milborn (1950), and later Kamiya (1972) [10], identified that the type of flow regime is dependent on the liquid flow rate $\dot{V}$, the cup's angular velocity Ω and the physical properties of the liquid, namely its viscosity μ, density ρ and surface tension σ.

In order to allow comparison between different operating conditions, the following non-dimensional quantities were defined by [10]:

$$\dot{V}^+ = \frac{\dot{V}}{r^3\,\Omega} \tag{1}$$

$$St = \frac{\mu^2}{\rho\, r\, \sigma} \tag{2}$$

$$We = \frac{\rho\,\Omega^2\, r^3}{\sigma} \tag{3}$$

The non-dimensional volume flow rate $\dot{V}^+$ relates the actual volume flow rate $\dot{V}$ to the radius r and the rotational speed Ω of the rotating element. The stability number *St* relates viscous forces to inertial and surface tension forces and the Weber number *We* is a measure of the relative importance of the fluid's inertia compared to its surface tension.

In their experiments, [10] proposed correlations for the transition volume flow rate from direct droplet to ligament formation, $\dot{V}_1^+$, and from ligament to sheet formation, $\dot{V}_2^+$.

$$\dot{V}_1^+ = 6.5\; We^{-1.161}\; St^{-0.0705} \tag{4}$$

$$\dot{V}_2^+ = 5.13\; We^{-0.789}\; St^{0.036} \tag{5}$$

However, although geometrically similar to the dimensions of a planet gear with a journal bearing, the test conditions investigated by [10] used angular velocities and liquid flow rates which are significantly lower than those prevailing on a planet gear in an epicyclic planetary gearbox. Extrapolated results may be invalid as they are no longer supported by actual test data.

The liquid disintegration modes observed on rotating disks are similar to those observed on rotating cups. However, the flow conditions at which the disintegration mode changes from droplet to ligament formation and from ligament to sheet formation are different. In contrast to a rotating cup, a rotating disk exhibits significant slip between the bulk flow of the liquid and the rotating surface. Thus, the angular velocity of the liquid is lower than that of the rotating disk. Hence, the transition from one disintegration mode to another occurs at higher Weber numbers.

A fundamental study of oil film disintegration at the rim of a rotating disk has been performed by [11]. The configuration was an abstraction of a typical droplet generating source in a jet engine bearing chamber. Hence, both geometrical and operational conditions were similar to those of a planet gear in an epicyclic planetary gearbox. Non-dimensional characteristic numbers were defined slightly differently compared to [10] as follows.

$$\dot{V}^+ = \frac{\rho\,\dot{V}^2}{\sigma\,d^3} \quad (6)$$

$$Oh = \frac{\mu}{\sqrt{\rho\,d\,\sigma}} \quad (7)$$

$$We^* = \frac{1}{8}\frac{\rho\,\Omega^2\,d^3}{\sigma} \quad (8)$$

The non-dimensional volume flow rate $\dot{V}^+$ relates the liquid's density and the actual volume flow rate $\dot{V}$ to the liquid's surface tension and the disk diameter *d*. The meaning of the Ohnesorge number *Oh* is equivalent to the meaning of the stability number *St* (equation 2). The modified Weber number *We** was defined with the rim diameter rather than the rim radius (equation 3).

Similar to [10], correlations for the transition volume flow rate from direct droplet to ligament formation, $\dot{V}_1^+$, and from ligament to sheet formation, $\dot{V}_2^+$, were obtained from experimental testing.

$$\dot{V}_1^+ = 0.0854\,Oh^{-0.9}\,We^{*-0.85} \quad (9)$$

$$\dot{V}_2^+ = 0.1378\,Oh^{-0.33}\,We^{*-0.435} \quad (10)$$

If the liquid attaches to the chamfer of the rotating gear and separates at the lower edge of the gear base (diameter d_1 in Figure 5), i.e. it follows flow path (b_1) in Figure 5, it would be expected to disintegrate in accordance with the observations made on spinning cups. However, if the liquid attaches to the chamfer of the rotating gear and separates at the upper edge of the gear base (diameter d_2 in Figure 5), i.e. it follows flow path (b_2) in Figure 5, it would be expected to disintegrate in accordance with the observations made on spinning disks.

NUMERICAL METHODS SUITABLE FOR MODELING EXTERNAL OIL FLOW FROM JOURNAL BEARINGS

In order to develop a comprehensive understanding of the external oil flow from a journal bearing, a two-component flow model is required. In recent years, several methods have been developed to numerically predict the behavior of air and oil flow mixtures. A fundamental issue is to accurately model the interface between the two fluid components as the physical properties of the fluids change. The resolution of the air-oil phase interface will therefore affect the modeling of the interaction between the phases and thus, also affect the accuracy of the flow behavior prediction.

The modeling approaches can be categorized according to their kinematic description. There are two different mathematical representations of fluid flow; the Lagrangian and the Eulerian approaches.

The Lagrangian approach keeps track of the location of individual fluid particles. A fluid particle's path is followed and identified by its position at any given time. The fluid particle's velocity is mathematically described by

$$\underline{u} = \underline{u}(x_0, t). \quad (11)$$

The velocity vectors form a field which allows pathlines to be reconstructed.

The Eulerian approach describes the flow field through its properties as a function of space and time. The velocity is mathematically described by

$$\underline{u} = \underline{u}(x, t), \quad (12)$$

where *x* is the position in the flow field and *t* the considered point in time. The velocity vectors form a field which represents streamlines.

Among the Lagrangian approaches, the Discrete Phase Model (DPM) and the Smoothed Particle Hydrodynamics (SPH) methods are currently of interest for solving this type of two-component flow. The Eulerian approaches that are typically used include the Eulerian method, Volume of Fluid (VoF) and Level-Set (LS) methods.

PRELIMINARY MODELING CONSIDERATIONS

Preliminary modeling methodology and CFD pre-processing considerations focused on the following main aspects:

a) The selection of an appropriate two-component flow model and, based on this, the selection of an appropriate grid generation approach,
b) the geometry of the domain to be investigated and
c) the boundary conditions applied to the numerical model.

At this stage of the research project, all of the three points mentioned above apply to a simplified, non-orbiting journal bearing with a circumferentially and axially constant lubricating gap height h_0 (Figure 5).

Based on its capabilities, the VoF method is deemed the most appropriate for initial simulations. The main advantages of this method lie in its ability to capture a wide range of flow regimes, i.e. droplets, ligaments, sheets and films, providing the computational grid is sufficiently fine. Compared to other methods with similar capabilities, i.e. the Eulerian method, the VoF method is computationally less expensive.

When using the VoF method, the computational grid requires certain properties. In a 3D space, the use of regular hexahedral cells, i.e. cells with an aspect ratio close to one, is preferred in order to achieve accurate surface reconstruction. This type of calculational cell can be generated using either a structured or an unstructured grid. The main advantage of a structured grid is that it is computationally more effective. However, its ability to represent complex geometrical features is limited. Considering the relatively simple geometrical shape of the domain addressed in the present study (Figure 4), a structured grid was deemed to be most appropriate.

Once an understanding of the external journal bearing flow field has been developed, available numerical methods will be reviewed and re-assessed for applicability.

As the gear is symmetric with regards to its rotational and its vertical axis, the geometry of the domain of interest (Figure 4) can be represented by a CFD model as follows:

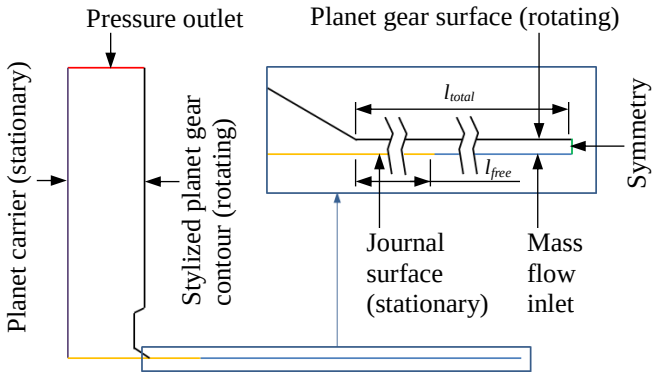

Figure 7: CFD model of domain of interest.

The journal (Figure 4) of the actual journal bearing has an axial groove, which typically extends over approximately 80% of the planet gear width, to supply oil into the lubricating gap. This feature is not symmetric to the rotational axis of the planet gear. However, a free inlet length, i.e. the distance between the mass flow inlet and the planet gear chamfer, of 10% of the planet gear width is more than sufficient for the flow to become fully developed in the axial and circumferential directions.

The CFD model shown in Figure 7 can be simplified (Figure 8). Based on the results of a single fluid component CFD model study of the inlet region, the free inlet length l_{free} was reduced to the actual distance required for the flow to become fully developed in the axial and circumferential directions. Thus, l_{free} could be reduced by a factor of two and the total inlet length l_{total} could be reduced by a factor of 11. This also reduces the number of computational cells in the simulation.

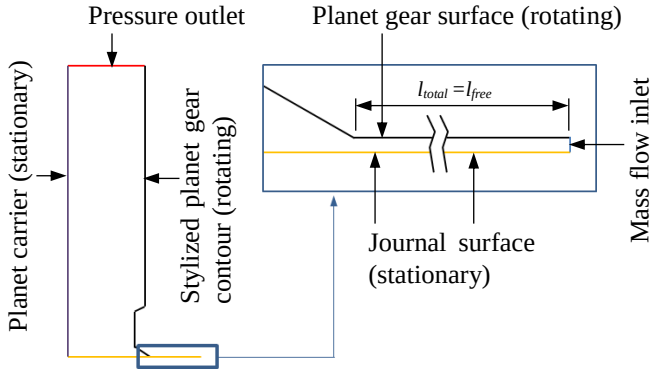

Figure 8: Simplified CFD model of domain of interest.

For preliminary investigations of the case considered it can be assumed that in steady state conditions the lubricating gap is completely filled with oil, i.e. is only occupied by a single fluid component. Therefore, having regular hexahedral cells for accurate interface reconstruction is a secondary requirement and cell aspect ratios can be increased to reduce the total cell count for the benefit of faster computation. A number of simple, single fluid component CFD models were set up and run in order to determine the maximum tolerable cell aspect ratio in the inlet region without compromising the accuracy of the numerical calculation. With h_0 being circumferentially and axially constant, this case was analyzed using an axi-symmetric model. The analysis concluded that an axial cell aspect ratio of 20 should not be exceeded.

INTERNAL AND EXTERNAL FLOW CHARACTERIZATION

Depending on the geometry and the operating conditions, the flow between two concentric rotating cylinders can be laminar or turbulent. The transition between the two flow regimes is preceded by flow instability. In a system with a rotating inner cylinder and a stationary outer cylinder parallel and centrifugal flow instability can occur [12].

Parallel flow instability is characterized by the Reynolds number *Re*. It relates inertial to viscous forces and can be calculated by

$$Re = \frac{\Omega\, d_{g,i}\, h\, \rho}{2\, \mu}. \tag{13}$$

The critical Reynolds number Re_{crit}, i.e. the Reynolds number which marks the transition from laminar to turbulent flow, is 2,000 [12].

Centrifugal instability can occur in flows with curved streamlines and is characterized by the Taylor number *Ta*. It relates centrifugal forces to viscous forces and can be calculated by

$$Ta = \frac{2\, h}{d_{g,i}} Re^2. \tag{14}$$

The critical Taylor number Ta_{crit} for the transition from laminar to turbulent flow is 1,708 [13]. With Ta_{crit} = 1,708 equation (14) can be rearranged for Re_{crit}.

$$Re_{crit} = 41{,}3 \left(\frac{d_{g,i}}{2\, h}\right)^{\frac{1}{2}} \tag{15}$$

It should be noted that centrifugal instability can only occur when the inner cylinder is rotating [13]. If, as in the present study, the inner cylinder (i.e. the journal) is stationary and the outer cylinder (i.e. the planet gear) is rotating, only parallel flow instability can occur.

The Reynolds number *Re* was calculated with the actual geometrical and operational values and fluid properties for the case under consideration. Based on the result, it can be concluded that the flow inside the lubricating gap is laminar.

Although the internal journal bearing oil flow is laminar, the external journal bearing flow may not be. Again, *Re* was calculated to characterize the flow regime in the external flow

domain (Figure 4). According to [14], for rotating disks, *Re* is calculated by

$$Re = \frac{\Omega\, r^2\, \rho}{\mu}. \qquad (16)$$

The Reynolds number *Re* was calculated with the actual geometrical and operational values and fluid properties for the case under consideration. Based on the result, it can be concluded that – at least at high cavity radii – the air flow will be turbulent. Therefore, a turbulence model has to be applied throughout the domain as a multi-zone treatment is currently not available in ANSYS Fluent [15].

A single fluid component CFD model was used to confirm the applicability of the *k-ω* Shear Stress Transport (SST) model inside the lubricating gap. According to [16], compared to other turbulence models, the *k-ω* SST model shows superior performance for wall-bounded boundary layers and low Reynolds number flows.

A plot of the predicted velocity profiles in the axial and circumferential directions indicated laminar flow behavior (Figure 9) with merged boundary layers. This is consistent with the expectation based on the calculated Reynolds number. The *k-ω* SST turbulence model is therefore adequate to simulate the laminar flow inside the lubricating gap.

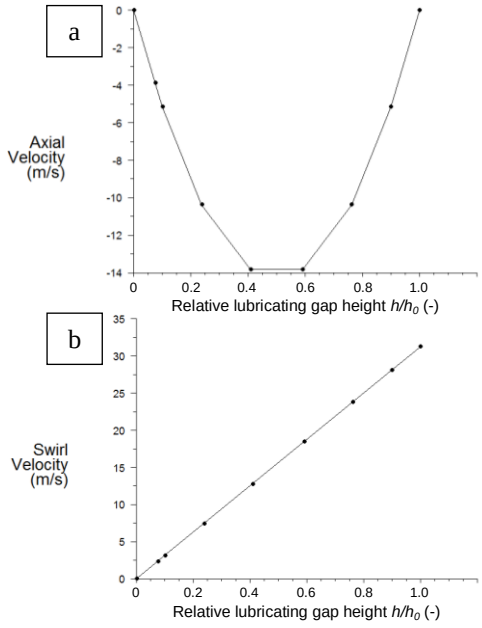

Figure 9: Fully developed velocity profiles in lubricating gap with *k-ω* SST turbulence model in the axial (a) and circumferential (b) directions.

Note that the standard k-ε turbulence model with scalable wall functions is inadequate to model this class of flow. Due to its formulation, it is only applicable to fully turbulent flows [17]. As a result, turbulent velocity profiles would have been predicted in the axial and the circumferential directions.

INITIAL CFD SECTOR MODEL RESULTS

Initial CFD analyses were performed at an oil temperature of *T*=30 °C. This temperature was used to simulate liquid properties similar to those of existing experiments and thus, enable comparison to flow behaviors observed on rotating disks and cups [8], [9], [10], [11]. It should be noted that this temperature is not representative of any typical journal bearing operating temperature.

Based on the knowledge gained from the preliminary considerations discussed in the previous section, an initial 3D, 10°, rotationally periodic sector model was created. The VoF method was used to track the air-oil phase interface. All key boundary conditions and parameter settings are listed in Annex A, Table 3. The computational mesh used for this model was created in a two dimensional (2D) space and subsequently rotated by +/- 5° around the bearing's axis. The initial mesh consisted of 9,200 cells in each 2D plane. The sector, in turn, consisted of 25 planes, resulting in a total cell count of 220,800.

With oil continuously entering the domain through the mass flow inlet (Figure 8), the phase interface progressively moves from the inlet boundary towards the planet carrier. When the oil exits the lubricating gap the axial velocity reduces rapidly due to the relatively high oil viscosity. Thus, the oil film thickness increases. In fact, the oil film thickness increases to such an extent that body forces are no longer negligible. The swirling oil is driven radially outward towards the gear chamfer. From there it follows the planet gear contour. The oil separates as a sheet which subsequently disintegrates into ligaments (Figure 10).

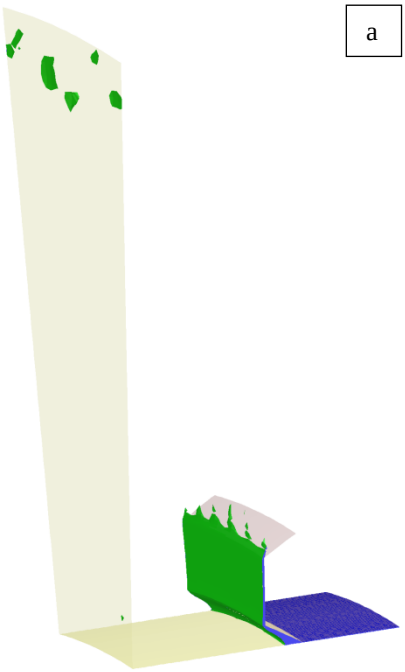

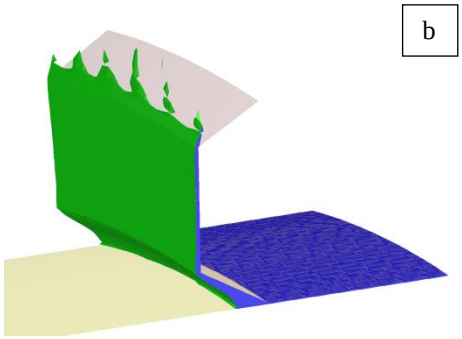

Figure 10: CFD sector model results for *T*=30 °C with boundary conditions and parameter settings as specified in Annex A, Table 3 in full view (a) and detail view (b). Displayed iso-surface indicates 50% cell oil volume content.

The simulated flow regime follows flow path (b_2) in Figure 5 and is therefore qualitatively comparable to flow regimes previously observed on rotating cups and disks.

Assuming that the simulated flow behaves like flow over a rotating cup [10] or disk [11], the expected flow regime can be determined by comparing the non-dimensional flow rate $\dot{V}^+$ with the transition flow rates $\dot{V}_1^+$ and $\dot{V}_2^+$. For $\dot{V}^+ < \dot{V}_1^+$ direct droplet formation is expected, for $\dot{V}_1^+ < \dot{V}^+ < \dot{V}_2^+$ ligament formation is expected and for $\dot{V}_2^+ < \dot{V}^+$ sheet formation is expected.

The characteristic numbers, i.e. $\dot{V}^+$, *St*, *We*, *Oh*, *We**, and the transition flow rates $\dot{V}_1^+$ and $\dot{V}_2^+$ were calculated with the actual geometrical and operational values and fluid properties for the case considered. Table 1 provides an overview of the calculated values.

Table 1: Characteristic numbers for initial CFD sector model for *T*=30 °C with boundary conditions and parameter settings as specified in Annex A, Table 3.

	Cup [9]	Disk [10]
Non-dimensional flow rate $\dot{V}^+$	8.10×10^{-04}	0.395
Reference equation	1	6
Transition flow rate from droplet to ligament formation $\dot{V}_1^+$	1.87×10^{-07}	5.91×10^{-06}
Reference equation	4	9
Transition flow rate from ligament to sheet formation	2.12×10^{-05}	6.16×10^{-04}
Reference equation	5	10
Result	$\dot{V}^+ > \dot{V}_2^+$	$\dot{V}^+ > \dot{V}_2^+$
Predicted flow regime	Sheet formation	Sheet formation

Table 1 shows that for the case considered, sheet formation is predicted as the liquid disintegration mode when compared to both rotating cups and disks. This is consistent with the results from the CFD simulation.

It should be noted that the characteristic numbers obtained for this specific case of journal bearing operation are outside the range of characteristic numbers investigated by [10] and [11]. However, since $\dot{V}^+$ is one and three orders of magnitude larger than the transition value, some confidence can be gained that the actual flow regime is in fact sheet formation.

The simulated flow pattern shown in Figure 10 is very regular, i.e. the ligaments released from the edge of the sheet are nearly equispaced. In order to confirm that this regularity is not imposed by the rotationally periodic boundary condition, a full 360° model was set up and run. The flow field behavior and the flow pattern proved to be very similar compared to that observed in the 10° sector model. Thus, it was concluded that a sector model is adequate to simulate external oil flow from a simplified, non-orbiting journal bearing with an axially and circumferentially constant lubricating gap height h_0.

MESH DENSITY STUDY

Post-processing of the initial CFD sector model results indicated poor resolution of the oil film thickness on the vertical gear face (Figure 10b). Finer meshes with improved resolution of oil-wetted near-wall regions were generated to assess the effect on the external journal bearing oil flow. Figure 11 (a, b_1, b_2, c) summarizes the key results from the mesh density study.

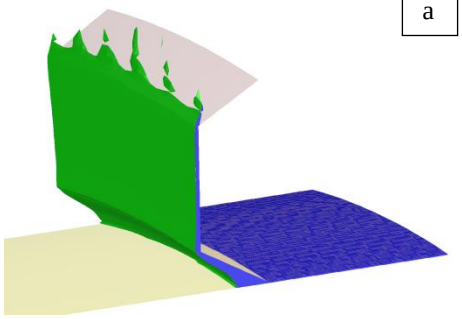

Sector size: 10°
$N_{cells,2D}$ =9.2k
$N_{cells,\phi}$ =24
$N_{cells,total}$ =221k
t_1 =0.100 mm
$N_{cells,oil,d1}$ =2
N_{lig}/10°=5
d_1: sharp edge

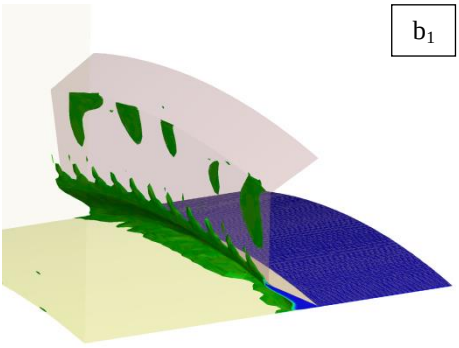

Sector size: 20°
$N_{cells,2D}$ =13.1k
$N_{cells,\phi}$ =59
$N_{cells,total}$ =773k
t_1 =0.010 mm
$N_{cells,oil,d1}$ =8
N_{lig}/10°=5
d_1: sharp edge

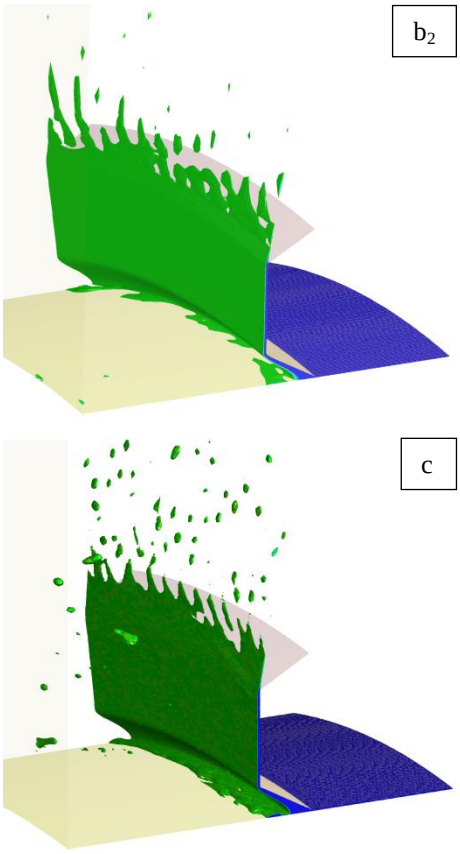

Figure 11: CFD sector model results for T=30 °C with boundary conditions and parameter settings as specified in Annex A, Table 3 for different mesh densities. Displayed iso-surface indicates 50% cell oil volume content.

The study concluded that the general flow regime is relatively insensitive to the mesh density. With the exception of the flow regime shown in Figure 11b$_1$ the oil always follows flow path (b$_2$) in Figure 5. For the case shown in Figure 11b$_1$, further investigations are required to identify the root cause as to why exactly the flow separates from the lower edge of the gear base (diameter d_1 in Figure 5).

The initial geometry featured sharp edges in areas where two or more faces meet. It was anticipated that this would lead to an adverse pressure gradient particularly around the sharp edge of diameter d_1 (Figure 5). For this reason, the very same mesh density and characteristics used to simulate the external oil flow shown in Figure 11b$_1$ were used to simulate the oil flow with a 0.3 mm fillet radius applied to the lower edge of the gear base (diameter d_1 in Figure 5). The result is shown in Figure 11b$_2$. With a 0.3 mm radius present, the oil flow stays attached to the gear contour until it separates as a sheet from the upper edge of the gear base (diameter d_2 in Figure 5). Both meshes with higher and lower densities did not show this sensitivity, i.e. the predicted flow path (flow path (b$_2$) in Figure 5) was identical irrespective of a 0.3 mm radius being present or not.

As shown in Figure 11, the mesh density affects the number of ligaments in the modeled sector. The number of ligaments is of interest as this will affect the size of the droplets generated by ligament disintegration. A small number of large ligaments will generate bigger droplets than a high number of small ligaments. A separate study was performed to assess the dependency of the number of calculational cells in the circumferential direction $N_{cells,\phi}$/10° on the number of ligaments N_{lig}/10° (Table 2). The computational mesh used for this analysis was the 2D mesh used to simulate the external oil flow shown in Figure 11b$_1$.

Table 2: Effect of number of cells around circumference $N_{cells,\phi}$/10° on number of ligaments in sector N_{lig}/10° with a 2D mesh density of $N_{cells,2D}$ =13.1k cells.

$N_{cells,\phi}$/10°	29.5	59.5	119
N_{lig}/10°	6	11	19

A strong dependency between $N_{cells,\phi}$/10° and N_{lig} /10° can be concluded.

CFD SECTOR MODEL RESULTS WITH ELEVATED OIL TEMPERATURE

At elevated oil temperatures the liquid properties, namely density ρ, viscosity μ and surface tension σ, will change. Of these properties, oil viscosity is most strongly affected by a change in temperature.

The three different mesh densities and characteristics previously used to simulate external oil flow at a temperature of T=30 °C (Figure 11a, 11b$_1$ and 11c) were used to simulate the external oil flow at an elevated temperature of T=70 °C. This temperature was chosen as the value for the oil viscosity reduces by a factor of five.

An oil temperature equivalent to Maximum Take-Off (MTO) conditions has also been assessed. Although the oil temperature at MTO conditions is significantly higher than T=70 °C, it was concluded from the CFD simulations that the general flow regime observed at T=70 °C is similar to that observed at T=T_{MTO}.

With oil continuously entering the domain through the mass flow inlet (Figure 8), the phase interface progressively moves from the inlet boundary towards the planet carrier. When the oil exits the lubricating gap the oil film continues to progress towards the planet carrier. Due to lower internal fluid friction, as a result of the lower viscosity, the reduction of the oil film's axial velocity is less abrupt than previously observed at an oil temperature of T=30 °C. Hence, the oil film thickness is reduced and the liquid continues to travel axially along the journal surface in a swirling motion. When the oil film's axial velocity does reduce slightly, the film thickness increases and thus, the effect of the centrifugal force acting on the oil film becomes more significant. Ligaments, which are formed on the advancing oil front, are driven radially outward and in axial

direction (Figure 12). If the flow simulation runs for a sufficiently long elapsed time, the oil film will reach the planet carrier and completely cover the journal surface. The simulated flow regime follows flow path (a) in Figure 5.

Figure 12 shows the predicted oil flow behavior for T=70 °C with boundary conditions and parameter settings as specified in Annex A, Table 3. The model used a mesh which consists of 13.1k cells in each 2D plane. The 20° sector, in turn, consists of 60 planes, resulting in a total cell count of $N_{cells,total}$ =773k (Figure 11b$_1$).

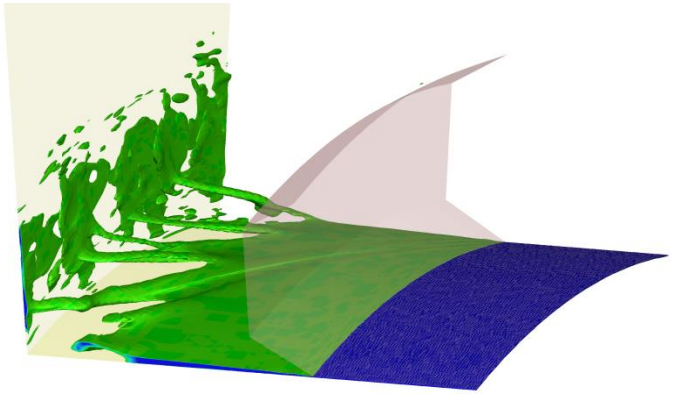

Figure 12: CFD sector model results for T=70 °C with boundary conditions and parameter settings as specified in Annex A, Table 3. Displayed iso-surface indicates 50% cell oil volume content. Mesh with $N_{cells,total}$ =773k (Figure 11b$_1$).

The predicted flow behavior is independent of the mesh density, i.e. the oil always follows flow path (a) in Figure 5.

Similar to the observations made at an oil temperature of T=30 °C, the mesh density affects the number of ligaments in the sector. The three different mesh densities investigated revealed a very similar dependency between the number of cells in circumferential direction, $N_{cells,\phi}$/10°, and the number of ligaments in the sector, N_{lig}/10°.

CONCLUSIONS FROM CFD ANALYSES

The CFD analyses carried out to date allow the following conclusions to be drawn.

a) A sector model is adequate to simulate the external oil flow of a simplified, non-orbiting, journal bearing with an axially and circumferentially constant lubricating gap height h_0.
b) At low oil temperature, i.e. high oil viscosity, the predicted oil flow path is relatively insensitive to the grid resolution. In all cases the exiting oil flow either followed flow path (b$_1$) or (b$_2$) in Figure 5. The coarsest and the finest meshes predict the same flow regime and oil flow path.
c) At low oil temperature, i.e. high oil viscosity, some grid resolution levels predict an oil flow path which is sensitive to the micro geometry of diameter d_1, e.g. 0.3 mm radius or sharp edge. More work is required to identify the root cause of this behavior.
d) The number of ligaments generated in a sector strongly depends on the number of cells in circumferential direction. This conclusion is independent of the oil temperature level used.
e) At higher oil temperature, i.e. lower oil viscosity, the predicted flow regime is independent of the mesh density used. All mesh densities used predict the same oil flow path (flow path (a) in Figure 5).
f) The oil viscosity affects the external flow behavior profoundly, i.e. the predicted flow path changes significantly.

OUTLOOK

In order to achieve the future objectives of creating a design tool for routine use and providing boundary conditions for a larger CFD model to simulate the oil scavenge behavior inside a planetary gearbox, the simplified model used for the CFD analyses in the present contribution will be extended.

In the first step, the model fidelity will be enhanced to include the orbiting motion of the journal bearing to better represent the kinematic conditions in an epicyclic gearbox. In order to separate key underlying physical phenomena, the model will continue to have an axially and circumferentially constant lubricating gap height h_0.

In the second step, radial bearing eccentricity, caused by external gear forces, will be included to fully represent a true journal bearing. CFD analyses will be carried out with and without orbiting motion.

Experimental rig testing is planned to be carried out in order to validate the simplified CFD model with an axially and circumferentially constant lubricating gap height h_0.

ACKNOWLEDGMENTS

This work has been carried out in collaboration with Rolls-Royce plc and is part of the Aerospace Technology Institute (ATI) MAMOTH research program.

Rolls-Royce plc's permission to publish this work is greatly appreciated.

The authors additionally acknowledge the support by ANSYS Inc.

Very valuable support has been provided by the University of Nottingham's Gas Turbine and Transmissions Research Centre (G2TRC), which is also home to the Rolls-Royce University Technology Centre (UTC) in Gas Turbine Transmission Systems, the Fluids and Thermo-Fluids departments of Rolls-Royce plc and Rolls-Royce Deutschland Ltd & Co KG, and the Structures and Transmissions department of Rolls-Royce plc.

REFERENCES

[1] Rolls-Royce plc Ultrafan™ engine with epicyclic gearbox, accessed 16 November 2016, < https://www.flickr.com/photos/rolls-royceplc/14151477988/in/album-72157644584413758/>.

[2] Townsend, D. P., 1991, "Dudley's Gear Handbook", 2nd edition, McGraw-Hill.

[3] Karaman, T., 1921, "Über Laminare und Turbulente Reibung", Zeitschrift für angewandte Mathematik und Mechanik, Vol. 1, No. 4.

[4] Daily, J.; Nece, R., 1958, "Roughness and Chamber Dimension Effects on Induced Flow and Frictional Resistance of Enclosed Rotating Disks", Massachusetts Institute of Technology.

[5] Dorfman, L. A., 1963, "Hydrodynamic Resistance and Heat Loss of Rotating Solids", Oliver & Boyd.

[6] Owen, J. M.; Rogers, R. H., 1989, "Flow and Heat Transfer in Rotating-Disc-Systems – Volume 1: Rotor-Stator Systems", Taunton: Research Studies Press Ltd.

[7] Reynolds, O., 1886, "On the Theory of Lubrication and its Application to Mr. Beauchamp Tower's Experiments, including an Experimental Determination of the Viscosity of Olive Oil", Philosophical Transactions of the Royal Society of London, Vol. 177, page 154 to page 234.

[8] Fraser, R. P. et al, 1963, "The Filming of Liquids by Spinning Cups", Chemical Engineering Science, Vol. 18, page 323 to page 337.

[9] Hinze, J. O.; Milborn, H., 1950, "Atomization of Liquids by Means of a Rotating Cup", ASME Journal of Applied Mechanics, Vol. 17, page 145 to page 153.

[10] Liu, J. et al, 2012, "Experimental Investigation of Liquid Disintegration by Rotary Cups", Chemical Engineering Science, Vol. 73, page 44 to page 50.

[11] Glahn, A. et al, 2002, "Droplet Generation by Disintegration of Oil Films at the Rim of a Rotating Disk", Journal of Engineering for Gas Turbines and Power, Vol. 124, page 117 to page 124.

[12] Szeri, A. Z., 1980, "Tribology: Friction, Lubrication and Wear", Hemisphere Publishing Corporation.

[13] Taylor, G. I., 1923, "Stability of a Viscous Liquid Contained between Two Rotating Cylinders", Series A, Containing Papers of a Mathematical or Physical Character 223.605-615, page 289 to page 343.

[14] Theodorsen, T.; Regier, A., 1944, "Experiments on Drag of Revolving Disks, Cylinders, and Streamline Rods at High Speeds", NACA Report 793.

[15] ANSYS Inc., 2013, "ANSYS Fluent User's Guide".

[16] ANSYS Inc., 2006, "Modeling Turbulent Flows", Introductory Fluent Training.

[17] ANSYS Inc., 2013, "ANSYS Fluent Theory Guide".

ANNEX A

Table 3: CFD model key boundary conditions and parameter settings

Parameter	Value/setting
Numerical solver	ANSYS Fluent 16
Multi-phase model	VoF (explicit)
Energy model	Isothermal
Turbulence model	k-ω SST
Air density (30 °C)	1.165 kg/m^3
Air dynamic viscosity (30 °C)	1.87×10^{-05} kg/(ms)
Air density (70 °C)	1.029 kg/m^3
Air dynamic viscosity (70 °C)	2.06×10^{-05} kg/(ms)
Oil density (30 °C)	985.3 kg/m^3
Oil viscosity (30 °C)	0.047 kg/(ms)
Oil density (70 °C)	957.3 kg/m^3
Oil viscosity (70 °C)	0.009403 kg/(ms)
Surface tension model	Enabled
Surface tension (30 °C)	0.03158 N/m
Surface tension (70 °C)	0.02858 N/m
Rotational speed of gear	$\Omega = \Omega_{MTO}$
Rotational speed of carrier and journal	0 rad/s
Inlet type	Mass flow inlet
Air inlet mass flow rate	0 kg/s
Oil inlet mass flow rate	$\dot{m}_{oil} = \dot{m}_{oil,MTO}$
Outlet type	Pressure outlet
Spatial discretization volume fraction	Geo-reconstruct

